Science Advances
AAAS

Supplementary Materials for

Therapeutic strategies targeting uPAR potentiate anti–PD-1 efficacy in diffuse-type gastric cancer

Long Qin, *et al*.

Corresponding author. Zuoyi Jiao, jiaozy@lzu.edu.cn; Qi Wang, wangqi09sysu@gmail.com; Jing Yang, yangjing0502@aliyun.com

Sci. Adv. **8**, eabn3774 (2022)
DOI: 10.1126/sciadv.abn3774

This PDF file includes:

Supplementary figures and figure legends

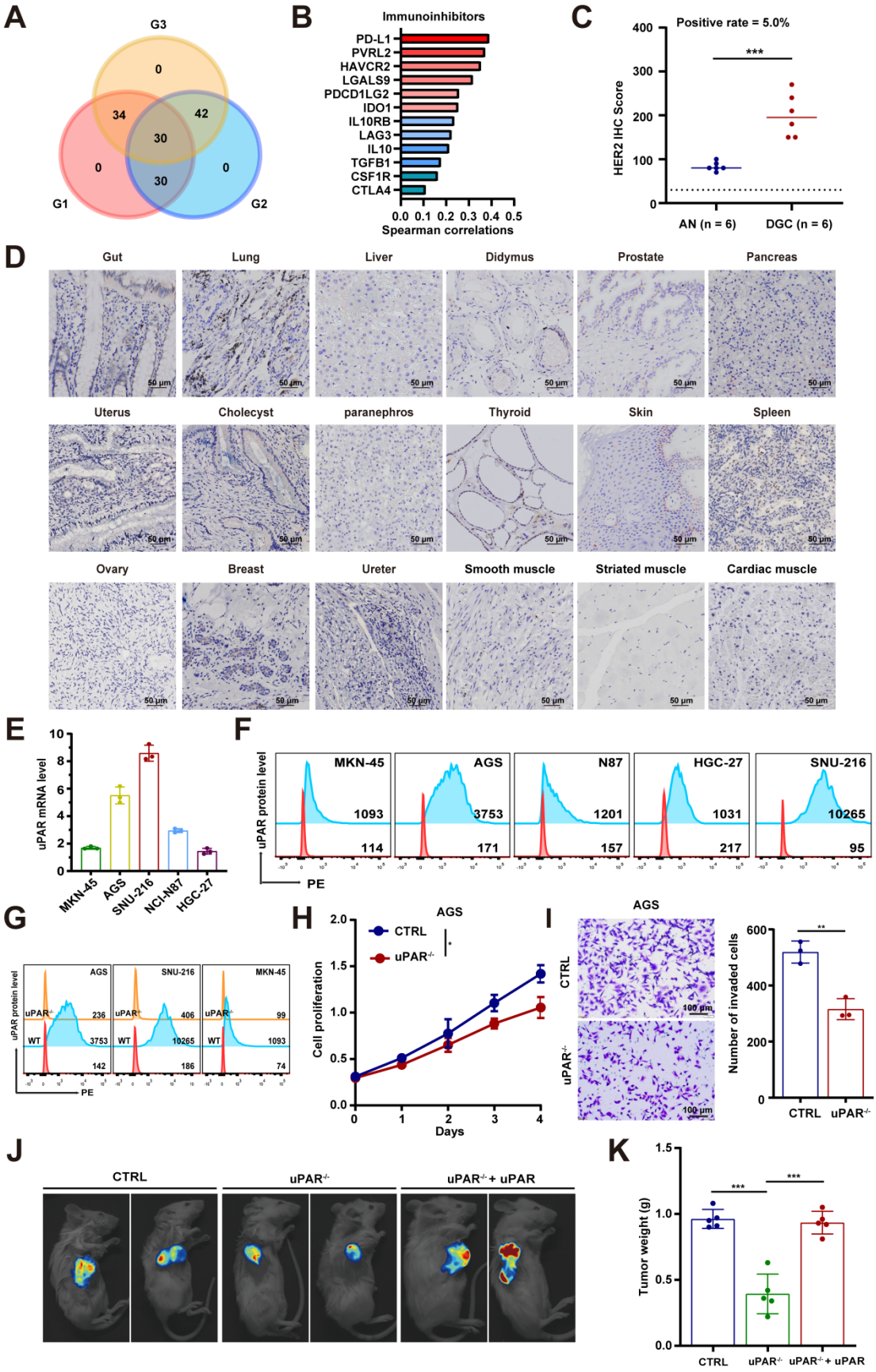

fig. S1. Related to Fig 1. (A) Venn diagram showing the number of proteins found to be differentially expressed in the tumors from 15 DGC patients (n = 5/group, 3 groups). uPAR was detected in all 3 groups. (B) Analysis of correlation between uPAR and immunosuppressive genes using the TISIDB database. (C) HER2 positivity rate in DGC patients (6/121) defined by IHC score 3+ with ≥ 10% of the cells showing positive reactivity. (D) IHC analysis of uPAR protein levels in human vital organs. (E and F) uPAR mRNA (E) and protein (F) levels in GC cell lines shown by qRT-PCR and flow cytometry. (G) uPAR knockout efficiency in GC cell lines shown by flow cytometry. (H) Growth curves of AGS ctrl and *uPAR*$^{-/-}$ cells. (I) Transwell invasion assay of AGS ctrl and *uPAR*$^{-/-}$ cells. (J and K) Bioluminescent imaging (J) and tumor weight (K) of NSG mice carrying wild type, *uPAR*$^{-/-}$ or *uPAR*$^{-/-}$ complemented with *uPAR* MKN-45 cell line-derived xenografts at 19 dpi. Data are expressed as the mean ± SEM (* $p < 0.05$, ** $p < 0.01$, *** $p < 0.001$).

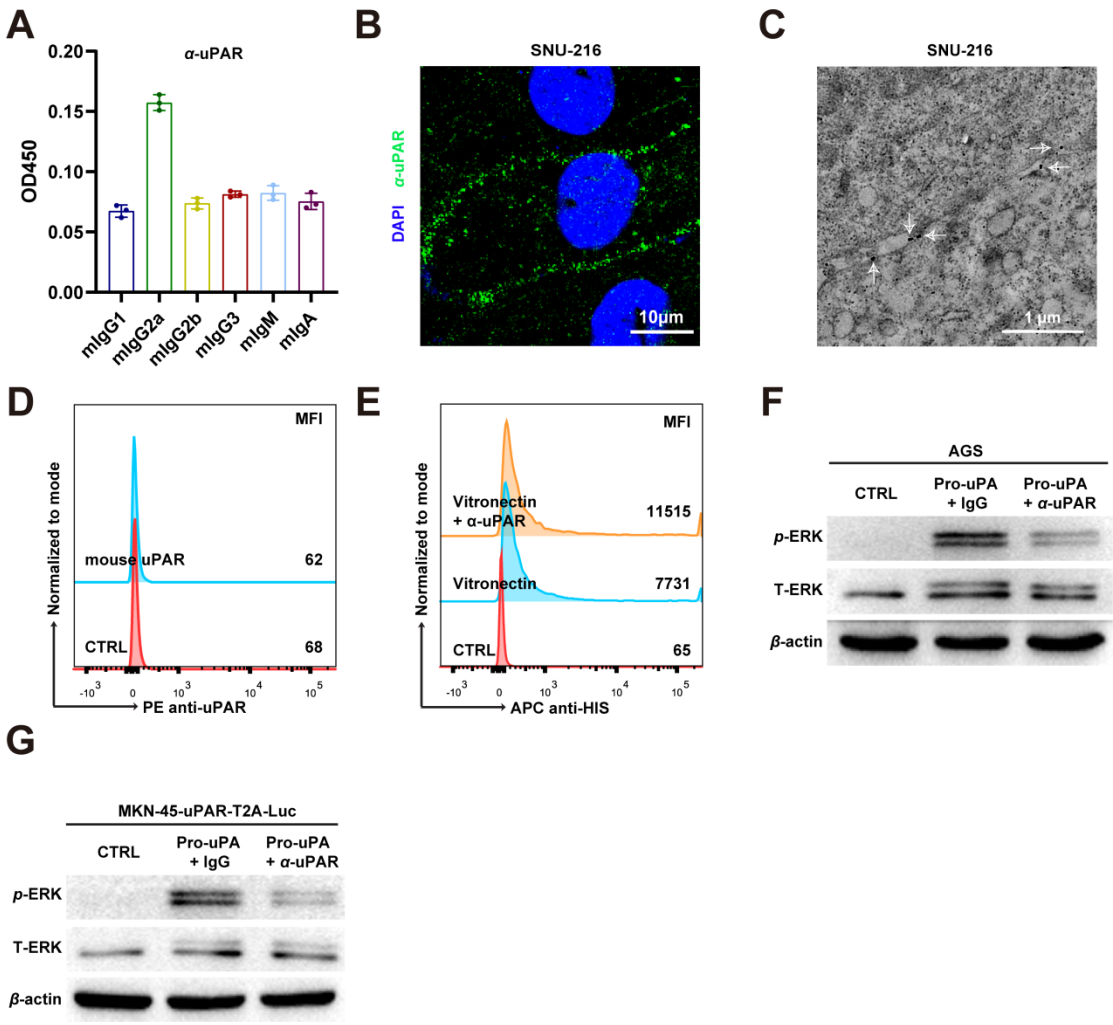

fig. S2. Related to Fig 2. (A) Antibody isotyping of the anti-uPAR mAb by ELISA. (B and C) IF (B) and immunoelectron microscopy (C) analysis of anti-uPAR binding to SNU-216 cells. (D) Negative binding of the anti-uPAR mAb to mouse uPAR shown by flow cytometry. (E) Competitive binding assay showing no inhibition of vitronectin (VN) binding to uPAR by the anti-uPAR mAb detected by flow cytometry. (F and G) Western blotting of phosphorylated ERK (*p*-ERK) and total ERK (T-ERK) in AGS and MKN-45-uPAR-T2A-Luc cells pretreated with anti-uPAR or ctrl mAb after pro-uPA stimulation.

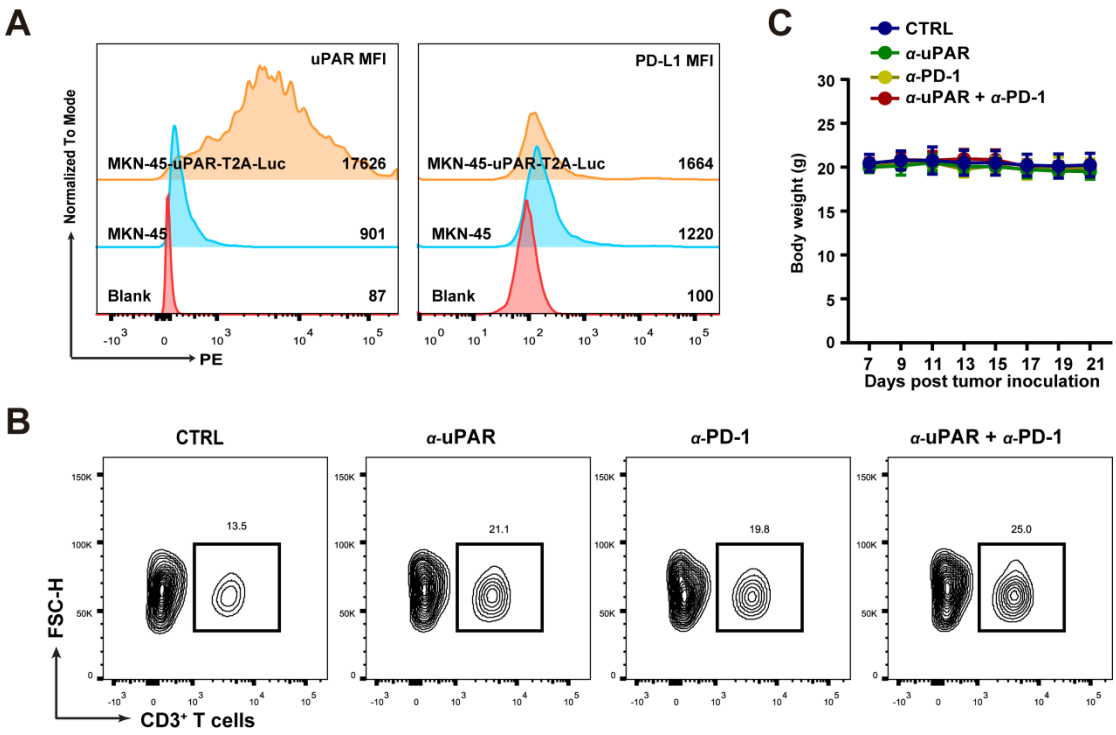

fig. S3. Related to Fig 3. (A) uPAR and PD-L1 protein levels in MKN-45 and MKN-45-uPAR-T2A-Luc cells shown by flow cytometry. (B) Frequencies of human T ($CD3^+$) cells in peripheral blood of the CDX mice at 21 dpi , as shown by flow cytometry. (C) Body weight of the CDX mice over the course of the experiment.

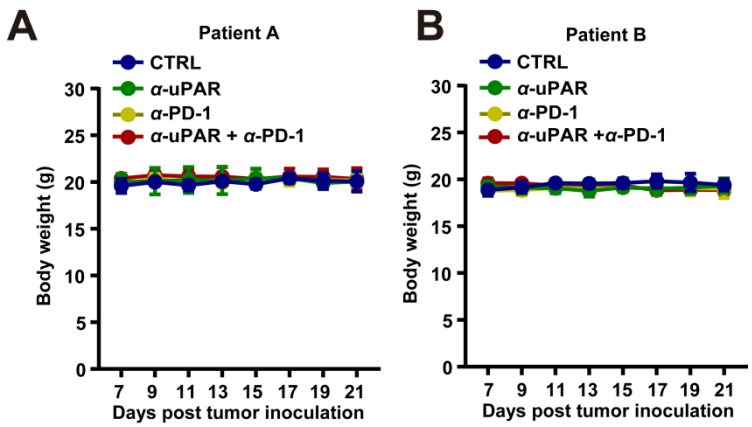

fig. S4. Related to Fig 4. (A and B) Body weight of mice bearing the PDX derived from patient A or B over the course of the experiment.

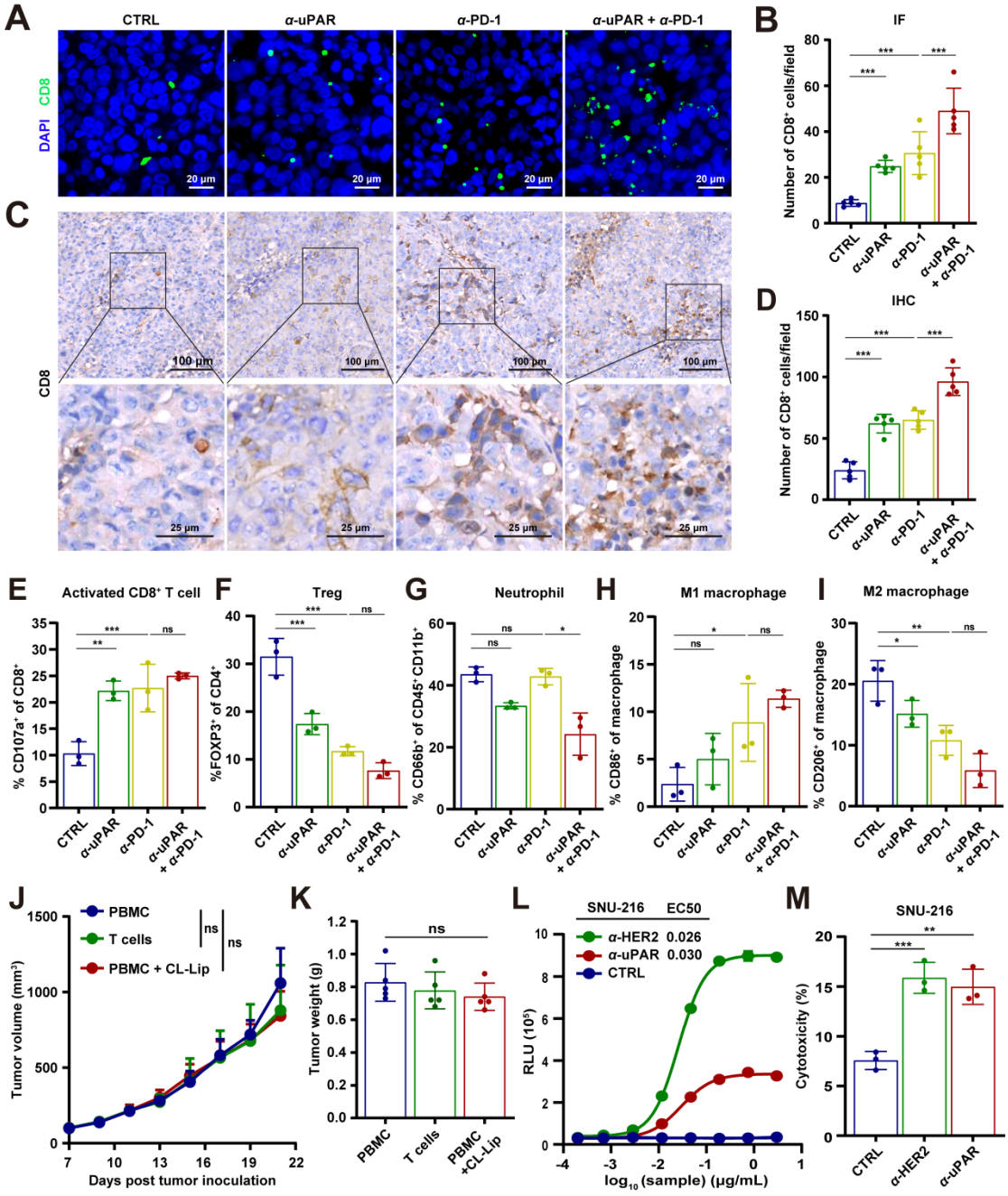

fig. S5. Related to Fig 5. (A and B) IF staining (A) and quantification (B) of $CD8^+$ T cells in the MKN-45-uPAR-T2A-Luc cell line-derived xenografts at 21 dpi. (C and D) IHC staining (C) and quantification (D) of $CD8^+$ T cells in the same CDX as in (A and B). (E to I) Frequencies of activated cytotoxic T cells ($CD45^+CD8^+CD107a^+$) (E), regulatory T cells (Tregs) ($CD45^+CD4^+FOXP3^+$) (F), neutrophils ($CD45^+CD11b^+CD66b^+$) (G), M1 macrophages ($CD45^+CD11b^+CD68^+CD86^+$) (H) and M2 macrophages ($CD45^+CD11b^+CD68^+CD206^+$) (I) in the MKN-45-uPAR-T2A-Luc cell

line-derived xenografts treated with different antibodies at 21 dpi, as shown by flow cytometry. (J and K) Tumor growth curves (J) in the MKN-45-uPAR-T2A-Luc cell line-derived xenograft mice (n = 5 per group) receiving normal hPBMCs (5×10^6 per mouse, I.V. injection), purified human T cells (2×10^6 per mouse, I.V. injection) or hPMBCs together with clodronate liposomes (CL-Lip, 0.2 mL for a young adult mouse of 20 grams, I.V. injection), an efficient reagent for the selective depletion of monocytes. (K) Tumor weight of the mice at 21 dpi. (L) ADCC assay using SNU-216 cells cocultured with Jurkat FcγRIIIa (158V) effector cells in the presence of ctrl, anti-HER2 or anti-uPAR mAb. (M) CDC assay showing the cytotoxicity of ctrl, anti-HER2 or anti-uPAR mAb on SNU-216 cells, detected by flow cytometry. Data are represented as mean ± SEM (ns nonsignificant, * $p < 0.05$, ** $p < 0.01$, *** $p < 0.001$).

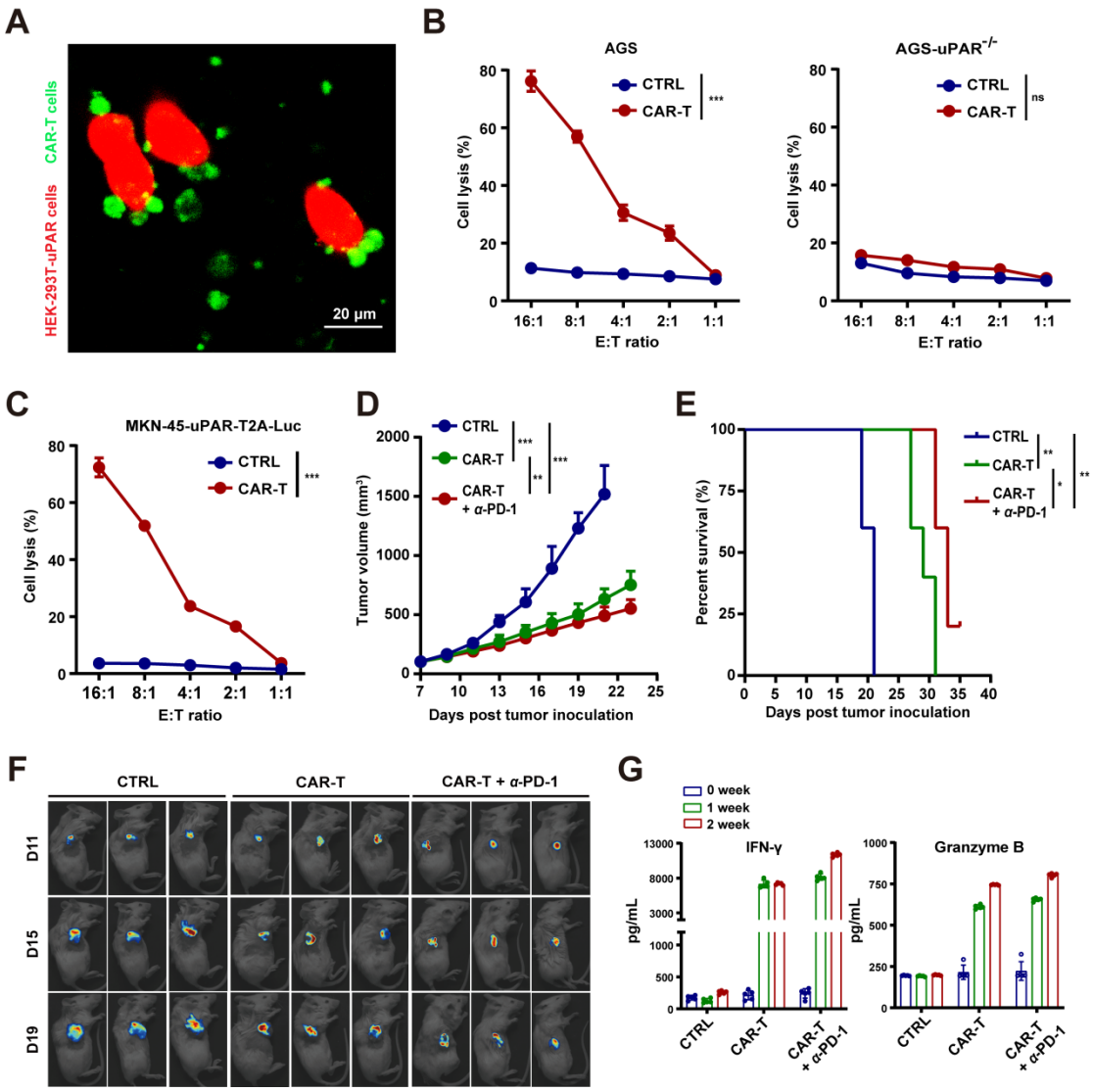

fig. S6. Related to Fig 6. (A) IF analysis of the binding of uPAR CAR-T cells (green) to uPAR-expressing HEK-293T cells (red). (B) Killing efficiency of AGS ctrl or *uPAR*$^{-/-}$ cells by uPAR CAR-T cells, determined by LDH-based cytotoxicity assay. (C) Killing efficiency of MKN-45-uPAR-T2A-Luc cells by uPAR-CAR-T cells, determined by luciferase-based assay. (D and E) Tumor growth (D) and survival (E) curves of the CDX mice treated with uPAR CAR-T or ctrl cells alone, or uPAR CAR-T cells plus anti-PD-1 (n = 5 per group; uPAR CAR-T or ctrl cells 2×10^6, I.V., only once 7 dpi; anti-PD-1 mAb 10 mg/kg, I.P., every 5 days starting from 8 dpi). (F) Bioluminescent imaging of the CDX mice in (D and E) at different days post tumor inoculation. (G) Protein levels of IFN-γ and granzyme B in the serum of CDX mice at different weeks post tumor inoculation detected by ELISA. Data are represented as mean ± SEM (ns nonsignificant, * $p < 0.05$, ** $p < 0.01$, *** $p < 0.001$).

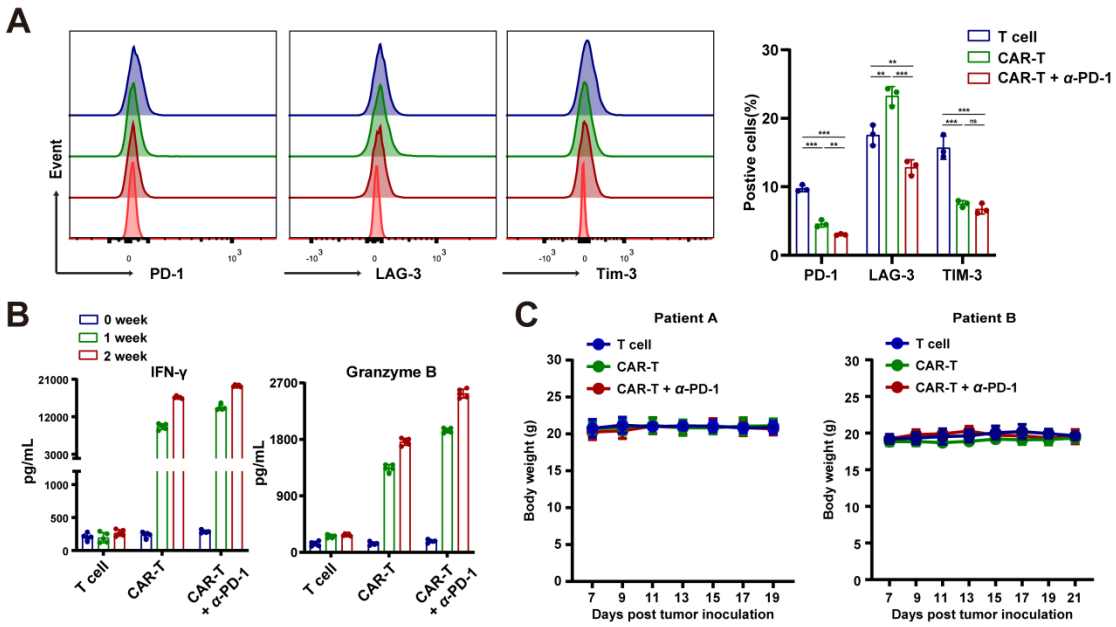

fig. S7. Related to Fig 6. (A) Protein levels of PD-1, LAG-3 and TIM-3 in tumor-infiltrating lymphocytes at 21 dpi in the PDX mice (related to patient A) that received different treatments, as shown by flow cytometry. (B) Protein levels of IFN-γ and granzyme B in the serum of PDX mice (related to patient A) at different weeks post tumor inoculation detected by ELISA. (C) Body weight of mice bearing PDX derived from patient A or B over the course of the experiment. Data are represented as mean ± SEM (ns nonsignificant, ** $p < 0.01$, *** $p < 0.001$).

table S1. Clinical characterisics of patients A and B.

Clinical characterisics	patient A	patient B
Age (year)	53	57
Gender	male	male
Serum protein	TP (63.7 g/L) ALB (39.7 g/L) AFP (1.57 ng/ml) CEA (1.12 ng/ml) CA125 (5.95 U/ml) CA199 (206.60 U/ml) CA72-4 (-)	TP (58.3 g/L) ALB (41.6 g/L) AFP (1.80 ng/ml) CEA (2.40 ng/ml) CA125 (5.92 U/ml) CA199 (<2.00 U/ml) CA72-4 (<1.50 U/ml)
Neoadjuvant chemotherapy regimen	Two cycles of FLOT	None
Operation date	2020.08.18	2020.09.10
Operation style	Laparoscopic conversion to open distal gastrectomy	Laparoscopic total gastr-ictomy
Operation time (min)	155 min	270 min
Tumor location	Lower third	Upper third
Tumor size	2.0 x 2.0 x 1.0 cm	3.5 x 3.0 x 0.7 cm
Lauren classification	Diffuse type	Diffuse type
TNM stage	T4N3M0	T4N1M0
Immunohistochemistry	CKp (+) CK8/18 (+) LMP-1 (-) C-erbB-2 (-) PMS-2 (+) MLH-1 (+) MLH-6 (+) MSH-2 (+) Syn (-) CD20 (-)	CKp (+) CK8/18 (+) LMP-1 (-) C-erbB-2 (-) PMS-2 (+) MLH-1 (+) MLH-6 (+) MSH-2 (+) Syn (-) CD20 (-)
Ki67	60%	70%
Postoperative chemotherapy regimen	Two cycles of FLOT	One cycle of XELOX
Postoperative Survival (month)	6 (dead)	17 (alive)

table S2. Sequences of the guide RNAs (gRNAs) used for CRISPR/Cas9-mediated *uPAR* knockout

Target	Sequences (5'-3')
gRNA I	GAAGATCACCAGCCTTACCG(AGG)
gRNA II	TTCCACACGGCAATCCCCGT(TGG)
gRNA III	GGACCACGATCGTGCGCTTG(TGG)

table S3. Primer sequences used for qRT-PCR.

Gene	Sequences (5'-3')
GAPDH-Forward	GGAGCGAGATCCCTCCAAAAT
GAPDH-Reverse	GGCTGTTGTCATACTTCTCATGG
uPAR-Forward	GGGGATTGCCGTGTGGAAGAGT
uPAR-Reverse	CTTCAAGCCAGTCCGATAGCTCAGG
CCL3-Forward	AGTTCTCTGCATCACTTGCTG
CCL3-Reverse	CGGCTTCGCTTGGTTAGGAA
CCL4-Forward	TAGATTACTATGAGACCAGCAGC
CCL4-Reverse	TCAGTTCAGTTCCAGGTCATACA
CCL5-Forward	CCAGCAGTCGTCTTTGTCAC
CCL5-Reverse	CTCTGGGTTGGCACACACTT
CXCL9-Forward	TGCAAGGAACCCCAGTAGTG
CXCL9-Reverse	AGGGCTTGGGGCAAATTGTT
CXCL10-Forward	GTGGCATTCAAGGAGTACCTC
CXCL10-Reverse	TGATGGCCTTCGATTCTGGATT
CXCL11-Forward	GACGCTGTCTTTGCATAGGC
CXCL11-Reverse	GGATTTAGGCATCGTTGTCCTTT